



Practical computational modeling of the structure and its bracing system for the design of primary metal building frames

Bálint Vaszilievits-Sömjén¹, Aakash Reddy
Eetikala², Donald W. White³

Abstract

In current practice, the primary frames of metal buildings are typically designed using planar 2D structural analysis. The frame is considered laterally restrained out-of-plane by the connected secondary structural elements, such as purlins, girts and flange diagonal bracing. The points of connection of these secondary members typically are assumed to act as fully braced for the design of the primary framing. The secondary elements must meet the stiffness and strength requirements specified in AISC 360-22 Appendix 6 to qualify as suitable bracing elements per AISC 360.

However, satisfying the existing bracing stiffness requirements can lead to challenges, particularly in buildings where the roof purlins support standing seam roof panels and in large-span buildings where ordinary bracing systems may not be sufficient.

This paper demonstrates an approach to the above design problem focusing on direct modeling of the primary structure using thin-walled open-section beam theory frame elements along with the direct modeling of the out-of-plane restraint from the bracing system (purlins, girts, flange diagonal bracing, wall and roof panels, and the building longitudinal bracing). The structural analysis for the force demands on the primary structure still focuses on the 2D planar response, while the overall stability assessment focuses on the 3D system behavior. The proposed method calculates and uses elastic critical load multipliers to predict the corresponding global buckling strength of the stabilized members. The results from the proposed approach are compared and contrasted with other design-based calculations.

1. Lateral-torsional buckling strength of members stabilized by bracing not fulfilling full bracing stiffness requirements - Introduction

When evaluating the lateral-torsional buckling (LTB) strength of a member using the formulas outlined in Chapter F of the AISC 360 *Specification* (AISC, 2022), a primary dependent variable is the unbraced length (L_b). This crucial metric is defined as the distance between points either braced against lateral displacement of the compression flange or braced against the twist of the cross-section. The potential use of an LTB effective length factor to account for the influence of boundary conditions is discussed in the Commentary to the *Specification*.

¹ Senior Research Engineer, Consteel Solutions Ltd, Hungary <balint.vaszilievits@consteelsoftware.com>, PhD Student, Széchenyi István Egyetem, Győr, Hungary

² Graduate Research Assistant, Structural Engineering, Mechanics and Materials, Georgia Institute of Technology, <aetikala3@gatech.edu>

³ Professor, Structural Engineering, Mechanics and Materials, Georgia Institute of Technology, USA <dwhite@ce.gatech.edu>

However, the AISC 360 Appendix 6 stability bracing requirements focus on developing the calculated member strengths associated with the use of effective length factors $K = 1.0$.

To ascertain whether a member qualifies for the use of L_b in the determination of its strength, the connected bracing must meet the stiffness and strength criteria specified in Appendix 6 of AISC 360. These requirements, formulated to provide practical solutions for prevalent situations in routine steel structures, present challenges in the context of load-bearing portal frames in metal buildings. This is due to peculiarities uncommon in many other steel structures, including:

- Utilization of web-tapered and general non-prismatic members.
- Incorporation of purlins and girts attached only to the outside member flange for lateral stabilization, while the member is exposed to combined axial compression and major-axis bending.
- Implementation of torsional restraint through flange diagonal braces connecting the inside flange to the purlins or girts, while the member being exposed to combined axial compression and major-axis bending.
- Use of roof systems that cannot be classified as rigid in their plane, hence not providing full lateral support at each purlin line for the roof girder.

Due to these distinctive characteristics, there arises a need to explore alternative approaches that are compatible with the nuances of metal buildings and allow for improved assessment of the bracing system stiffness and strength. It would be useful to develop a design methodology capable of easily predicting a member's LTB strength based on the provided stiffness and strength of the specified bracing system.

Appendix 6 of AISC 360 focuses predominantly on the bracing stiffness and strength requirements to develop the full-bracing strength of steel members (based on unbraced lengths subjected either to concentric axial compression in the absence of applied bending moment or applied bending moment in the absence of axial compression, using $K = 1$ for axial compression as well as for LTB). Appendix 6 aims to provide bracing design rules that are simple to apply for routine situations with members subjected solely to axial compression or bending. The Section 6.4 commentary to Appendix 6 provides limited recommendations for calculating the bracing stiffness and strength requirements for routine members subjected to combined axial compression and bending.

A significant focus of the AISC Appendix 6 bracing design rules is the provision of sufficient brace stiffness so that the second-order amplification of bracing displacements and forces is limited to levels that can be satisfied economically by routine bracing components. The challenge for the implementation of these rules in metal building design is their application for more complex bracing situations, including situations where certain bracing components may have relatively small stiffness.

The proposed solution addresses the stiffness requirements via practical computational modeling of the main metal building frames and their bracing systems. The engineer performs the member and bracing design given elastic eigenvalue buckling solutions using realistic models of the structure and its bracing system. The main frame members are designed for the in-plane force requirements obtained from a planar second-order elastic analysis based on the AISC direct analysis method. The bracing members are designed for force requirements provided by simple rules. In the following, first a design methodology based on the provided

bracing stiffness is presented. Second, a proposal for the determination of the bracing forces is discussed.

2. Use of the General Method for the design of structures with full bracing specified in accordance with stiffness requirements of Appendix 6.

The General Method, described in Vaszilievits-Sömjén, et al. (2023), is a methodology especially suited to the design of metal building frames. The General Method approach is closely related to the design procedures discussed in AISC/MBMA Design Guide 25 (White et al. 2021). In the examples presented by the above authors, the lateral bracing was assumed to be stiff enough and strong enough to fulfill the AISC 360 full bracing requirements. Therefore, the bracing was modeled using infinitely rigid out-of-plane lateral supports. Based on this condition, elastic linear buckling calculations were performed. The linear buckling eigenvalue problem then provided the elastic critical load multiplier used to determine the out-of-plane slenderness λ_{op} , equal to the square root of the ratio of the critical cross-section strength to the out-of-plane elastic buckling strength. The parameter λ_{op} is then employed as the fundamental dependent variable for the out-of-plane buckling strength verifications.

3. Recommended Approach - use of General Method for the design of structures considering the specific provided bracing characteristics and configuration

In the General Method of design, lateral supports can be readily modeled as springs representing the provided stiffness of the bracing system. The complete 3D structure can be modelled together with its bracing system, including the consideration of the membrane stiffness of the roof system. It is important to recognize that typical 12 DOF beam finite elements are not suitable for providing the elastic load multipliers used by this method. More advanced frame finite elements, including warping displacements, are necessary for such application.

3.1 Consequence of bracing stiffness on the LTB strength

Consider a fork supported member shown on Figure 2 with uniform cross-section subjected to a uniform bending moment along its length. In addition, consider a lateral point brace at the level of the upper flange, positioned at the mid-span. The distance between the end supports and the middle lateral support position is L_b .

The member strength based on L_b is valid if the bracing stiffness of the middle brace point is sufficiently high. In the AISC 360 procedures, the stiffness of a lateral brace is considered to be sufficiently high if the second-order amplification of any initial out-of-plane lateral displacement of the compressed flange at the brace point is limited to a factor of 2.0. Alternatively, AISC 360 also considers the bracing to be sufficient if solely a torsional brace having sufficient stiffness is provided at the brace point, restraining the rotation about the member's longitudinal axis. In this case, the overall lateral rigid-body movement of the cross section at the brace is unrestrained. For torsional bracing, the objective of the rules in AISC 360 is similarly to limit the amplification of any initial twist rotation of the brace point to a factor of 2.0. Recent research has shown that the prior AISC torsional bracing stiffness requirements generally need to be increased to meet this objective (Reichenbach et al. 2021). These increased requirements are largely due to the influence of lateral rigid-body movement of the member cross-section at the braced point.

In any case, when one conducts an elastic linear buckling analysis (ELBA) of the member and its bracing system, the above example member will buckle into a single wave pattern between its ends for smaller values of the bracing stiffness, and it will buckle into two half sine waves

with an inflection point and zero lateral displacement or twist at the middle brace for larger values of the bracing stiffness (see Figure 1). The smallest value of the bracing stiffness causing the member to buckle into two half sine waves (in this example) is referred to as the ideal bracing stiffness, β_i .

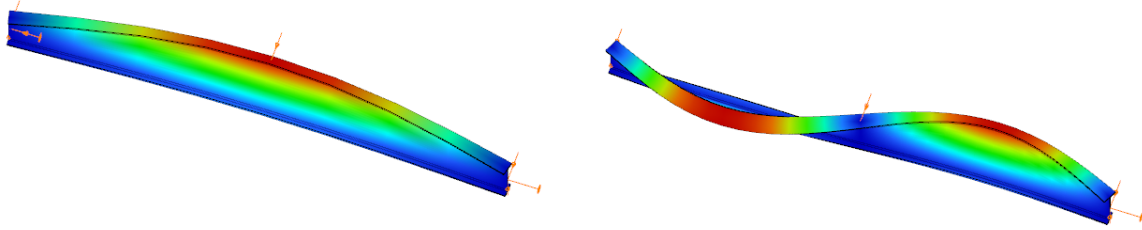


Figure 1: Buckling mode shapes in the case of a lateral brace with smaller or larger stiffness than the ideal bracing limit.

The use of the stiffness requirements of Appendix 6 ensures sufficiently high stiffness for routine bracing situations. These requirements aim for the use of bracing stiffnesses of at least $2\beta_i/\phi = 2\beta_i/0.75 = 2.67\beta_i$ for lateral bracing, and $3\beta_i/\phi = 3\beta_i/0.75 = 4\beta_i$ for torsional bracing (based in effect on the member inelastic or elastic LTB moment). If the bracing stiffness is larger than these minimum required values, used justify the use of L_b in LTB equation, the member is said to be fully braced and the LTB strength is assumed to be at its value based on rigid bracing.

In contrast, if the stiffness is smaller than Appendix 6 requirement, the physical member's LTB strength will tend to be reduced. The AISC 360 Appendix 6 provides a simple way of designing bracing systems with these smaller stiffness values. If the moment demand is smaller than the factored AISC member LTB strength based on L_b , the engineer is allowed to back-calculate a fictitious length that makes the factored flexural resistance equal to the moment demand. In contrast, Eurocode 3 (CEN, 2022) procedures consider the full bracing strength to be developed when the ideal bracing stiffness, β_i , is reached. The corresponding base Eurocode 3-member strength curves tend to be much more conservative than the AISC LTB strength curves, however.

If the bracing of the middle support does not meet the full bracing stiffness requirement under the current AISC Appendix 6 requirements, the engineer can conservatively neglect the bracing and calculate the LTB strength without considering its stabilization effect, thus employing $2L_b$ in the LTB design strength equations.

3.2 LTB strength considering lateral bracing not meeting the stiffness requirements.

The LTB strength corresponding to lateral brace stiffness varying between zero and the value for full bracing can be readily obtained by FEA simulation. The proposed General Method of design can be also applied by directly modeling stiffness of the bracing system.

Figure 2 shows a simply-supported member laterally restrained at its mid-span at its top flange. The member uses a welded I-section with the dimensions of a W21x44 and its unbraced lengths are $L_b = 10$ ft. The lateral stiffness of the brace is varied from zero to the full bracing stiffness based on AISC 360. As a result, the elastic eigenvalue will change as a function of the specified stiffness of the lateral brace.

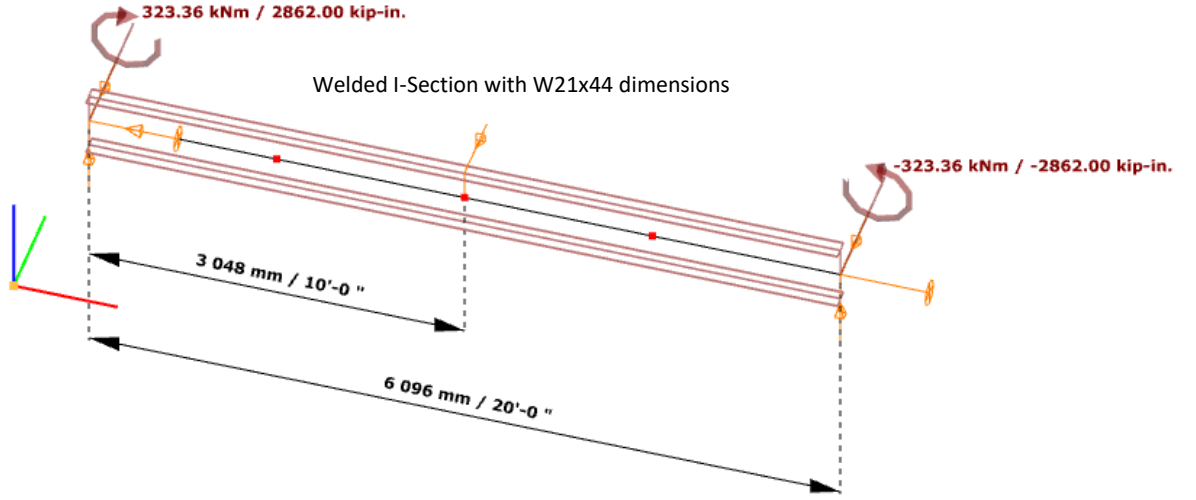


Figure 2: Simply-supported beam laterally braced at its mid-span.

Considering the variation of elastic eigenvalue as a function of the brace stiffness, the slenderness value λ_{op} defined as

$$\lambda_{op} = \sqrt{\frac{\gamma_{sg}}{\gamma_{e.op}}} \quad (1)$$

also changes. In this formula, γ_{sg} is the smallest cross-section strength-to-demand ratio and $\gamma_{e.op}$ is the out-of-plane elastic eigenvalue, see in Vaszilievits-Sömjén, et al. (2023).

In the application of the General Method in the context of the AISC 360 *Specification*, the LTB strength as a function of the slenderness λ_{op} can be written in the following form, similar to the LTB strength formulas in AISC/MBMA DG25 (White et al., 2021):

$$\text{For } \frac{M_L}{F_{yc} S_{xc}} < \frac{1}{\lambda_{op}^2} \leq 8.16$$

$$M_{nLTB} = R_{pg} R_{pc} M_{yc} \left[1 - \left(1 - \frac{M_L}{R_{pc} M_{yc}} \right) \left(\frac{\pi \lambda_{op} - 1.1}{\pi \sqrt{\frac{F_{yc} S_{xc}}{M_L} - 1.1}} \right) \right] \quad (2)$$

$$\text{and for } \frac{1}{\lambda_{op}^2} \leq \frac{M_L}{F_{yc} S_{xc}}$$

$$M_{nLTB} = \frac{R_{pg} M_{yc}}{\lambda_{op}^2} \quad (3)$$

The λ_{op} slenderness value, determined on a model that incorporates the actual provided stiffness of the bracing system, allows for a prediction of the strength of the member. This provides an alternative approach for design, applicable when the bracing elements do not satisfy the full bracing condition. It should be noted that the “plateau strength” for above example member, $R_{pg} R_{pc} M_{yc}$, is equal to the plastic moment, M_p . In addition, M_L is taken equal to $0.5M_{yc}$ as recommended by Slein et al. (2023) and Phillips et al. (2023a and b).

The following discussion compares the results from the above General Method calculation to the the results from a full nonlinear shell FEA in Abaqus (Simulia, 2024) for the member described in Figure 2. A sweep imperfection of the compression flange with an amplitude of $L_b/2000$ is specified in each of the unbraced lengths, and an out-of-alignment of the single mid-length brace point on the compression flange of $L_b/500$ is defined (see Figure 3). The one-half best-fit Prawel residual stress pattern is specified, which is representative of the residual stresses in welded I-section members (Slein et al. (2023), Phillips et al., (2023a and b)).

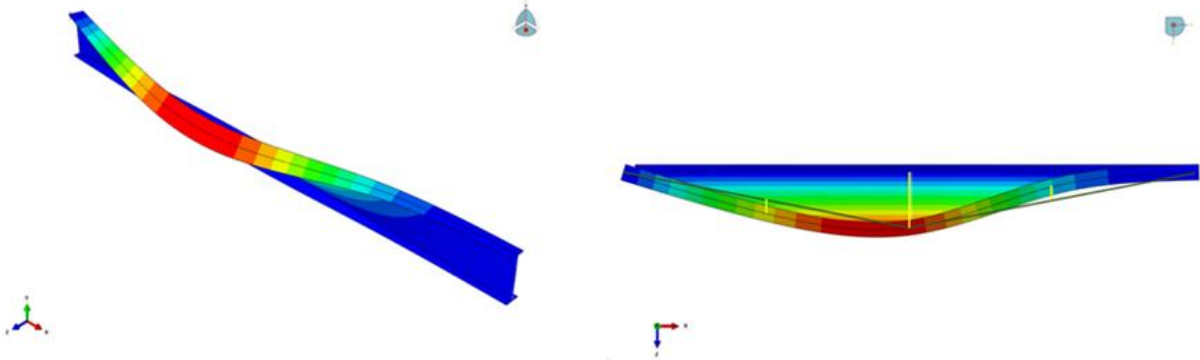


Figure 3: Initial imperfect geometry (contours indicate lateral displacement magnitude).

Figure 4 shows the ratio of the elastic critical moment to the member plastic moment, M_{cr}/M_p , the prediction by the General Method calculations based on the elastic eigenvalues for the different bracing stiffness values, M_n/M_p , and the strength determined from the FEA simulation, M_{FEA}/M_p . The FEA simulation strength starts at 29 % of the plastic moment for zero brace stiffness and asymptotically approaches 67% of the plastic moment as the bracing stiffness is increased. At the required AISC full bracing stiffness of $2.67\beta_i = 4(0.9)(3,185 \text{ kip-in})/20.3 \text{ in.}/120 \text{ in.}/0.75 = 6.27 \text{ kip/in}$, the FEA simulation shows that $0.67M_p$ is developed. Correspondingly, the General Method solution predicts a strength very close to the FEA simulation result for zero bracing stiffness, then a gradual increase in strength to the full-bracing value at $\beta_{br} = \beta_i$ (associated with ideal bracing for the elastic critical moment) approximately equal to $2(4,495 \text{ kip-in})/20.3 \text{ in.}/120 \text{ in.} = 3.69 \text{ kip/in}$. For β_{br} equal to this β_i , the General Method full-bracing strength is $0.68M_p$, whereas the FEA simulation indicates that the physical member would develop only 63% of its plastic moment strength. These are considered to be reasonable approximations.

If similar examples with other unbraced lengths are considered, the results are similar to those shown in Figure 6 for longer unbraced lengths where the LTB response is predominantly elastic. The General Method results tend to be slightly more conservative for shorter unbraced lengths, where the β_i based on developing the elastic critical moment becomes relatively large (due to the large value of the elastic critical moment relative to M_p). However, the General Method mapping from the elastic buckling moment to the design resistance still gives a reasonably accurate characterization of the FEA simulation results.

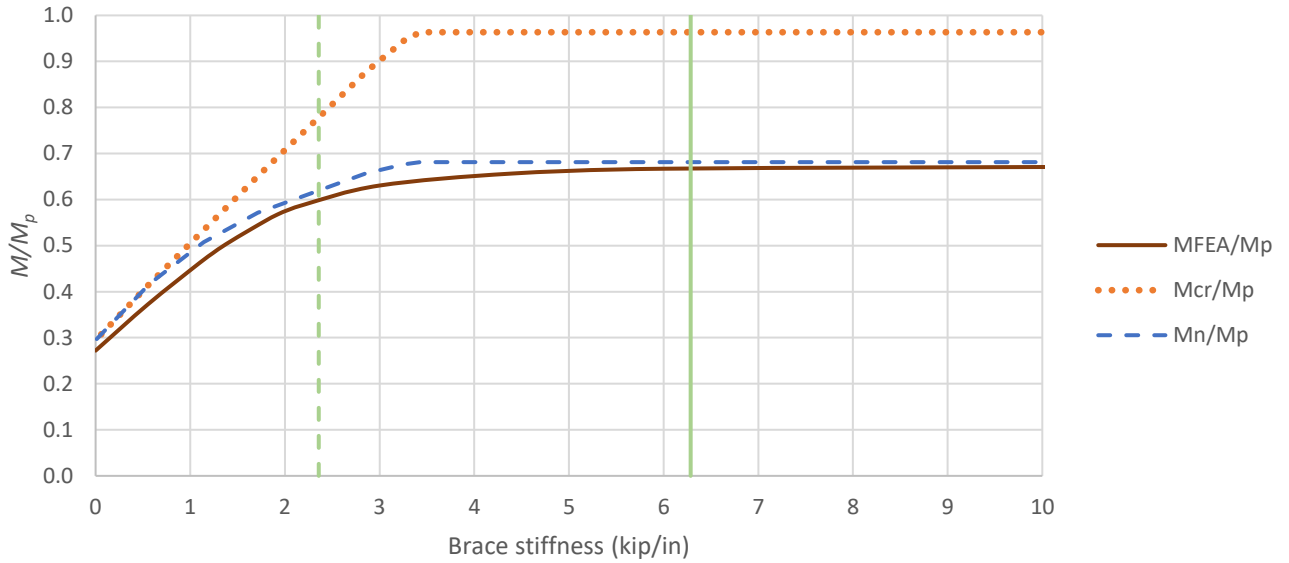


Figure 4: M/M_p as a function of the lateral brace stiffness.

Figure 5 shows the results for the above example member if a torsional brace is employed at its mid-span rather than a lateral brace. Web transverse stiffeners are employed at the brace location to prevent web distortion there. The torsional brace restrains the relative lateral displacement of the flanges but does not provide any restraint to overall lateral movement of the member cross section at the brace point. In this case, the FEA simulation indicates that at a torsional brace stiffness of $3\beta_i/\phi = 4\beta_i = 4[(0.9)(3,185 \text{ kip-in})]^2(240 \text{ in.})/29,000 \text{ ksi}/20.3 \text{ in.}^4 = 13,400 \text{ kip-in./rad}$, a member moment of only $0.62M_p$ is developed. However, the General Method solution suggests that the full bracing strength is achieved at β_i (associated with the elastic critical moment for full bracing) approximately equal to $(4,495 \text{ kip-in})^2(240 \text{ in.})/29,000 \text{ ksi}/20.3 \text{ in.}^4 = 8,240 \text{ kip-in./rad}$, where the FEA simulation indicates a nominal flexural resistance of $0.61M_p$. It is clear that the beam has difficulty reaching the theoretical full-bracing resistance in the FEA test simulation. This is due to the onset of rigid-body lateral displacement of the beam cross section at the brace point, even when the overall twisting of the cross-section at this point is highly restrained.

In spite of the limitations of the General Method in capturing the torsional bracing response in the above solution, one can argue that the General Method results do capture the overall trend in the strength gains with increases in the torsional bracing stiffness. The above AISC solution by the General Method can be improved by using an effective torsional brace stiffness of only one-fourth of the actual torsional brace stiffness. However, the FEA test simulation still indicates a strength of only $0.64M_p$ at a $\beta_{br} = 45,000 \text{ kip-in./rad}$. Therefore, the problem here is in part due to the fact that torsional bracing, in actuality, is not as efficient as lateral bracing in developing member flexural strengths.

Fortunately, for metal building frames, practically there is always some lateral bracing stiffness in addition to the torsional bracing stiffness at brace points employing diagonal braces from the girts or purlins to the inside flange of the member receiving the bracing (even if the stiffness of this bracing is very small, such as in the case of roof diaphragms composed of standing seam panels). Even a very small amount of lateral bracing stiffness provides significant help in avoiding the above difficulties (Prado and White, 2015).

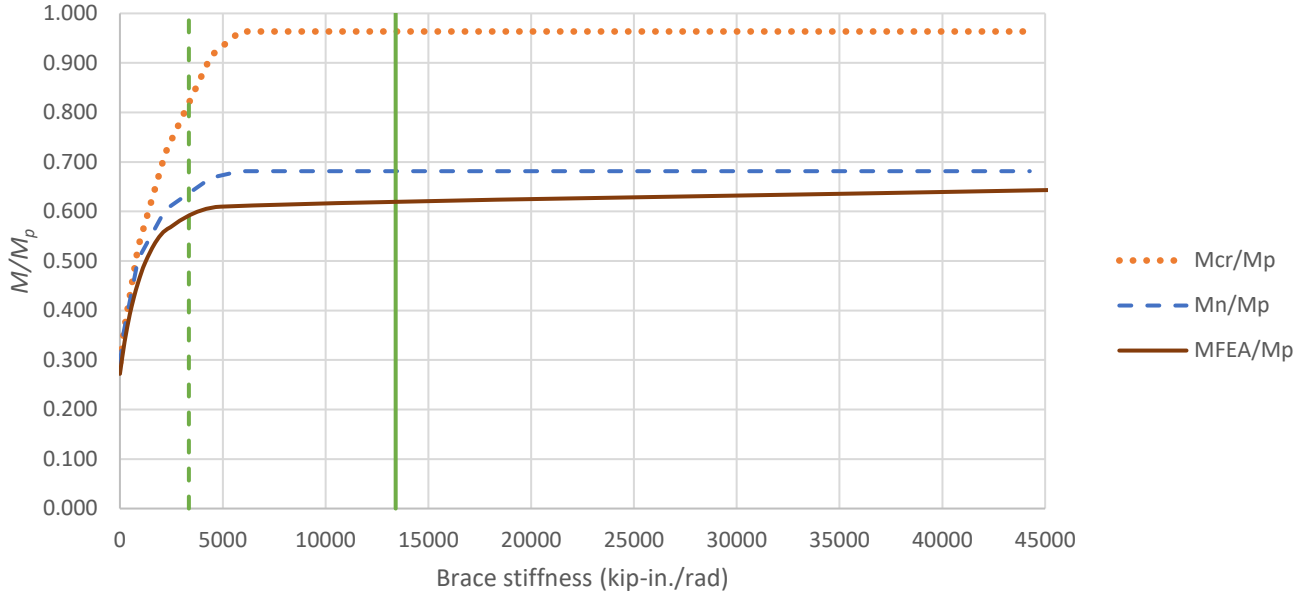


Figure 5: M/M_p as a function of torsional brace stiffness.

4 Determination of bracing forces

In general, the force requirements for the design of the bracing components can be obtained by performing a second-order analysis including appropriate geometric imperfections that tend to maximize the bracing force demands. However, the definition of geometric imperfections that will give safe worst-case estimates of the bracing forces is a complex task. Furthermore, these imperfections are strictly different for every bracing component within a given structure. Therefore, determination of bracing design forces directly from a second-order structural analysis with geometric imperfections often is prohibitive except for the simplest of structures (such as the example beam in Section 4).

Appendix 6 of the AISC 360 *Specification* provides simple algebraic equations defining representative worst-case bracing force requirements for routine cases with relatively simple bracing configurations and members subjected either solely to concentric axial compression or solely to bending moment. The Appendix 6 rules do allow for the use of a smaller bracing *stiffness* than that corresponding to full bracing when the member force demands are smaller than the member capacities based on the corresponding unbraced lengths with $K = 1.0$ (by allowing the engineer to calculate the brace stiffness requirement using a fictitious unbraced length that makes the member capacity equal to the corresponding force demand). However, there is no change to the bracing strength requirement equations in situations where these “partial bracing” stiffnesses are allowed. As noted in Section 1, the Appendix 6 Section 6.4 Commentary provides some guidance for determining the required bracing stiffness and strength for members subjected to combined axial compression and flexure. However, it should be noted that the Section 6.4 Commentary does not allow for the consideration of partial bracing conditions on beam-columns.

Fortunately, there are other options for addressing cases with partial bracing. Upon calculating the out-of-plane elastic buckling eigenvalue of metal building frames modeled in combination with their bracing systems, it is common for the $\gamma_{e.op}$ values to be larger than 2.0 for all the load combinations governing the design. As such, it can be argued that the second-order amplification of the bracing system displacements and forces will tend to be small. In these

cases, it should be possible to estimate the bracing system forces using simple approximations such as those recommended in Section 6.4 of the AISC 360 Appendix 6 Commentary.

In cases where the $\gamma_{e.op}$ values are less than than 2.0, it is recommended that the bracing system forces can be estimated conservatively by applying the amplifier.

$$\alpha = \frac{1}{1 - \frac{1}{\gamma_{e.op}}} \quad (4)$$

to the base bracing force requirements for rigid bracing (i.e., for $\beta_{br} = \infty$) to estimate the corresponding bracing force requirements. Studies by Prado and White (2015), Lokhande and White (2015), and White et al. (2011) suggest that the maximum bracing system forces at the member strength limit are rarely larger than 3 to 4 % of the corresponding member forces. Therefore, potentially a maximum cap on the amplified bracing component forces of 3 to 4 % may also be appropriate. However, further studies should be conducted to evaluate the appropriateness of such a maximum limit on the estimated bracing force demands.

Figure 6 shows an example of the lateral brace forces at the member maximum capacities for the example described in Figure 2, determined using the FEA test simulations associated with the strengths plotted in Figure 6. One can observe that even for a brace stiffness of approximately one-half of the ideal bracing stiffness, the bracing force is only 0.018 of the member M_n/h_o for the fully-braced member.

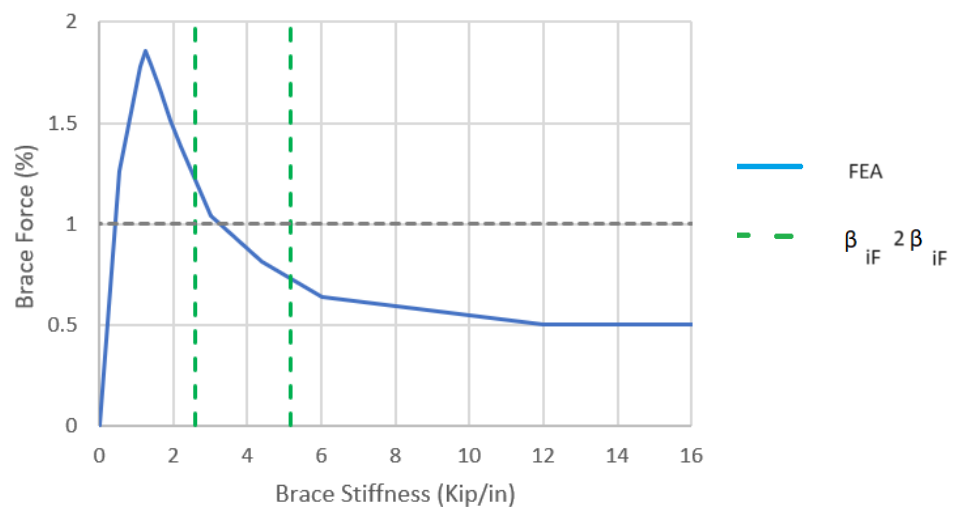


Figure 6: Plot of lateral brace stiffness vs brace force as a percentage of the moment capacity from full nonlinear shell FEA test simulation for the example beam.

5 Example Metal Building Frame

The following demonstrations were inspired by an example building provided by a leading North-American Metal Building company. The intermediate portal frame marked as ‘FL100’ in Figure 7 is evaluated using the proposed method.

In this structure, simply-supported portal frames with 80 feet span are laterally stabilized by the roof purlins connected to the outside flanges of its members. The purlins are made of cold-formed 8.5” deep Zee sections and carry two different roof system solutions: screwed-down trapezoidal sheeting and standing seam roof system. The frames are spaced at 25 feet.

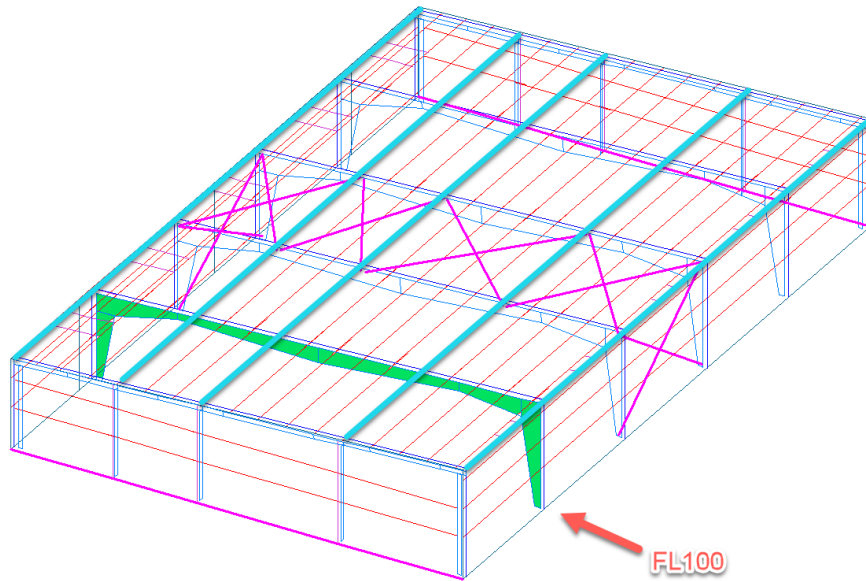


Figure 7: 3D layout of example metal building showing the position of the portal frame considered in this study.

The frame is evaluated for the LRFD gravity load combination $1.2D + 1.6L$ including the self-weight of the structure, a collateral load of 3.00 psf and a flat roof snow load of 21 psf.

In the case of the standing seam roof solution, no screws are used to fix the roof panels to the underlying purlins, to avoid the consequences of thermal movement. The attachments to the purlins are made with clips which allow the displacement of the panels in the direction parallel to their ribs within a specified range. As a consequence of this solution, the roof system lacks efficient lateral restraints to the purlins. In addition, the purlins can move relatively freely along their longitudinal direction, except those placed near the roof bracing nodes. The purlins with high translational flexibility cannot provide significant lateral restraint to the roof girder, only their bending stiffness can be considered in form of a torsional bracing for the girder. The torsional bracing is accomplished by adding flange diagonal braces.

In contrast, a conventional screwed-down roof typically exhibits high shear stiffness which in addition to stabilizing the purlins, ties them together. As such, all the purlins are able to provide lateral restraint to the roof girder, instead of only those located close to the nodes of the roof bracing. In addition to their lateral bracing role, they can provide torsional bracing to the roof girder at flange diagonal bracing locations. The flange diagonal braces provide lateral restraint to the inside flanges through the torsional stiffness provided by the roof purlins and by the attachments to the top flange, and in the case of the screwed-down roof panels, via the roof diaphragm stiffness. The flange diagonal braces are L-section members designed for compression and connected with bolts to the rafter and to the roof purlin.

The above complex mechanisms can be modelled readily and evaluated with the proposed method, employing special 14 dof frame finite elements. The solutions shown below are conducted using the Consteel (2024) software system. 3D models of the frame and its bracing systems are presented in which each bracing component is accurately represented with its actual stiffness.

5.1 Screwed-down roof option.

The 3D model shown in Figure 8 corresponds to the tributary area of the studied portal frame. In agreement with the proposed model by Wei et al. (2020), inflection points are assumed in the purlins at the boundaries of the tributary area. The ends of the purlins, modelled also with 14 DOF beam finite elements, are coupled to the rafter with equal displacement constraints so that the purlins deflect along with the in-plane deflections of the main frame.

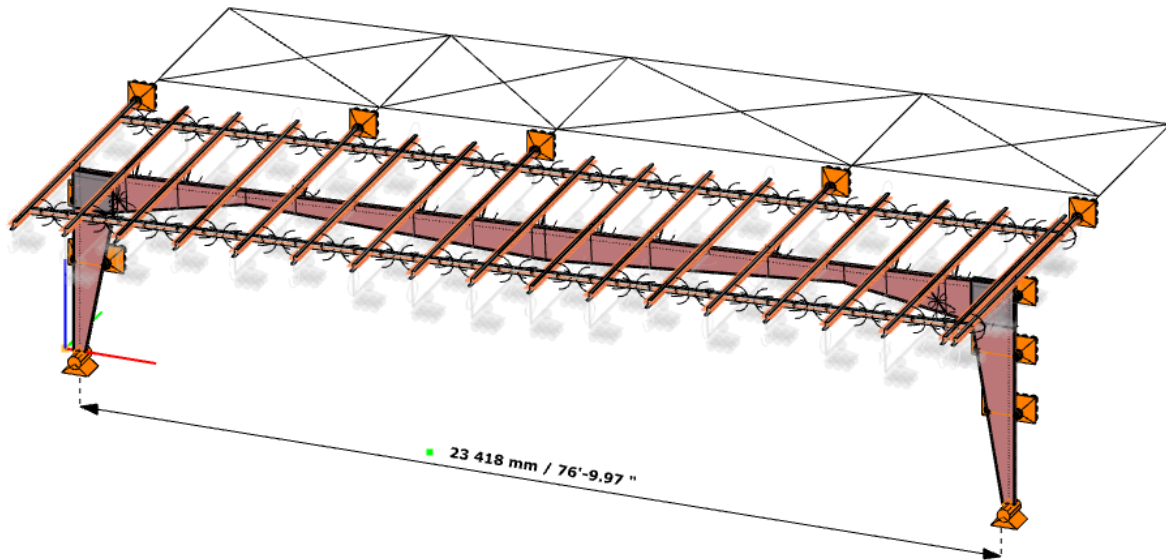


Figure 8: 3D model of the example portal frame with screwed-down roof panels.

To simulate the lateral stabilization of the purlins provided by the trapezoidal sheeting, special 1D line objects have been assigned to the top flange of each purlin, providing lateral and torsional restraint. The simulation of the effect of the sheeting's shear stiffness in the out-of-plane direction of the frame is realized by adding additional fictitious members between the purlins. These members are configured to represent the shear stiffness of the trapezoidal sheeting.

The utilized G' shear stiffness value of the sheeting is determined in accordance with AISI S310 (2020).

Those purlins which are placed close to the nodes of roof bracing are marked with support symbols in Figure 8. At these locations, for simplicity, infinitely rigid supports are assumed in the out-of-plane direction.

In the model the load is applied directly to the rafter, with the application points at the top of the rafter sections, thus considering the load-height effects (see Figure 9). The purlins are not directly loaded; they only serve to stabilize the main frame in this model.

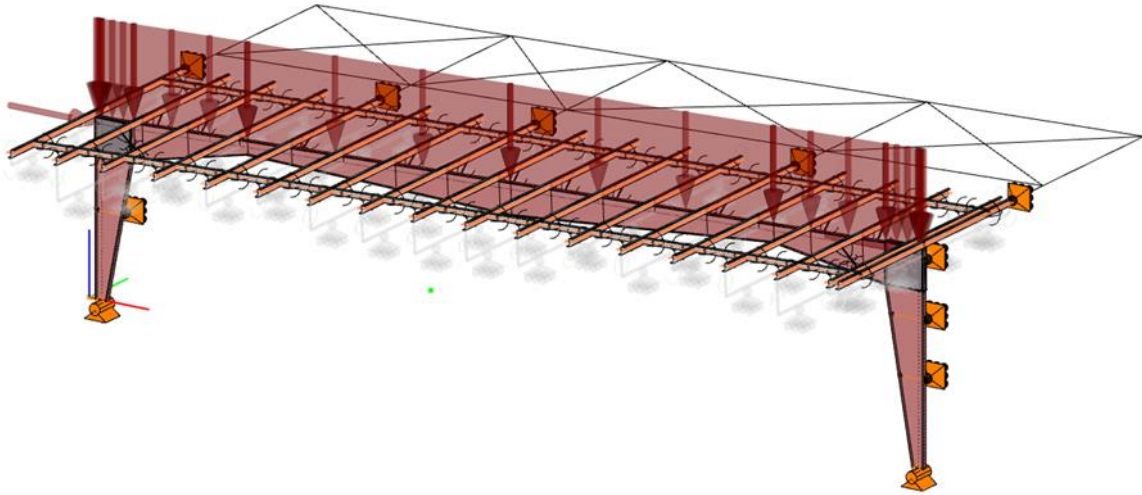


Figure 9: Load application on the frame.

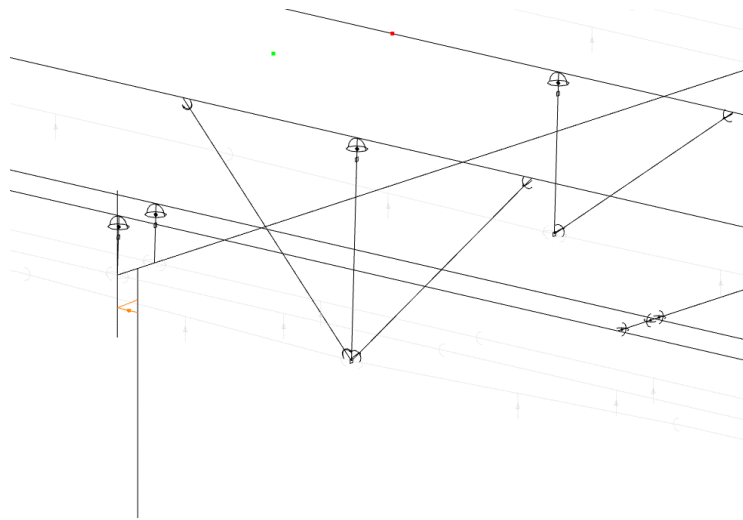


Figure 10: Line mode of the flange diagonal braces connecting the purlins to the bottom of roof girder at selected locations.

At locations where the inner flange is in compression from the gravity load combination, flange diagonal braces are used to connect the compressed flange to the purlins. The solution shown in Figure 10 is able to mobilize the flexural stiffness of the roof purlin and provide rotational restraint to the rafter.

The members representing the flange diagonal braces are also modelled with 14 DOF beam elements and are connected to the rafter by link elements to model their eccentricities.

The global buckling results are captured in the proposed λ_{op} slenderness, as discussed in Section 2. The slenderness values are determined from the elastic buckling eigenvalues of the global buckling solution. The mapping from the normalized slenderness to the member strength is made as described in Vaszilievits-Sömjén, et al. (2023) and summarized in Table 1.

Table 1: Mapping between slenderness and strength values.

Compression	Major-axis bending
$\lambda_{op}^2 < 2.25$	$\frac{M_L}{F_{yc} \cdot S_{xc}} < \frac{1}{\lambda_{op}^2} \leq 8.16$
$P_n = [0.658^{\lambda_{op}^2}] \cdot F_y \cdot A_e$	$M_{nLTB} = R_{pg} \cdot R_{pc} \cdot M_{yc} \left[1 - \left(1 - \frac{M_L}{R_{pc} \cdot M_{yc}} \right) \left(\frac{\pi \cdot \lambda_{op} - 1.1}{\pi \cdot \sqrt{\frac{F_{yc} \cdot S_{xc}}{M_L} - 1.1}} \right) \right]$
$\lambda_{op}^2 \geq 2.25$	$\frac{1}{\lambda_{op}^2} \leq \frac{M_L}{F_{yc} \cdot S_{xc}}$
$P_n = 0.877 \cdot \frac{F_y}{\lambda_{op}^2} \cdot A_e$	$M_{nLTB} = \frac{R_{pg} \cdot M_{yc}}{\lambda_{op}^2}$

Several ELBA buckling modes relevant for the verification of the rafter for combined compression and major-axis bending are shown together with the corresponding value of $\gamma_{e,op}$ in Table 2.

Table 2: Relevant elastic buckling modes for the frame with screwed-down roof panels.

Mode	$\gamma_{e,op}$	Elastic buckling mode shape
1	3.66	
3	4.57	
5	4.99	

The final unity check results, considering the interaction of axial compression and major-axis bending moments are evaluated in accordance with the AISC 360 Chapter H equations. Details for the performed calculations are explained in Vaszilievits-Sömjén, et al. (2023).

Figure 11 presents the unity checks on the main frame members. Since all the unity checks are below 1.00, the strength of the portal frame is sufficient to meet the demand.

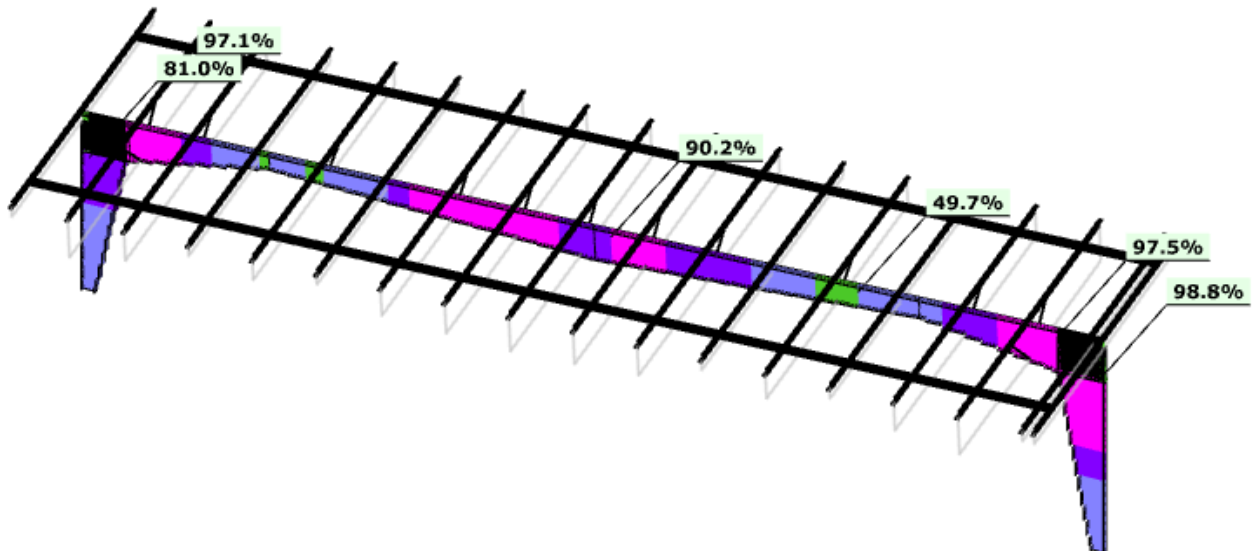


Figure 11: Final unity check results on the example portal frame with screwed-down roof panels.

5.2 Standing seam roof option

The modelling is made conceptually the same way as in the previous example for the frame with a standing seam roof (see Figure 12). However, there are some differences due to different characteristics of the roof systems that must necessarily be taken into account. For the proposed approach, it is assumed that the roof does not provide any shear membrane-type lateral restraint neither for the purlins nor for the rafter. The only stabilization effect provided by the sheeting is the bending stiffness of the clips connecting the sheeting to the roof purlins, which are modelled with spring support. It is important to note, that several standing seam solutions are available on the market, each having different characteristics. All solutions require an appropriate design solution. The example illustrated in this paper is not directly related to any of these actual solutions. The example is intended only to showcase the flexibility and capability of the design method.

The purlins placed close to the nodes of the roof bracing are supported by the same type of rigid supports as in the previous model for the screwed-down roof. The intermediate purlins marked with shaded support symbols on Figure 12 are not restrained longitudinally by the roof shear stiffness. Their displacement is restrained only by the flexibility of the special purlin clips with sliding connectors.

The flexibility of the clips can be determined from experimental tests. For this example, the values proposed by Wei et al. (2020), are used. The clips of the 24 in. wide roof panel are placed along the purlins with a spacing in accordance with the width of panel. The total number of clips used on the tributary area of the frame is $n_{cl} = 25 \cdot 12 / 24 = 12$ pieces, therefore the total stiffness provided against displacement in the direction perpendicular to the rafter is $\beta_{br} = n_{cl} \cdot k_c$

$= 12 \cdot 0.152 \text{ kip/in.} = 1.82 \text{ kip/in.}$ This value is considered in the form of an elastic spring support at the end of the purlins, marked with shaded support symbols on Figure 12.

Several ELBA buckling modes relevant for the LTB strength determination are shown in Table 3.

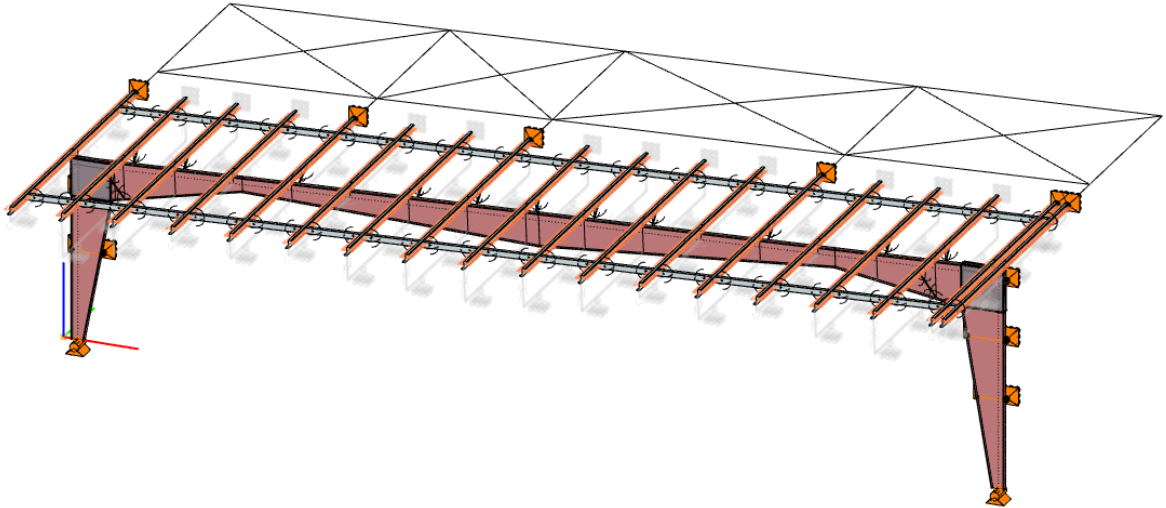
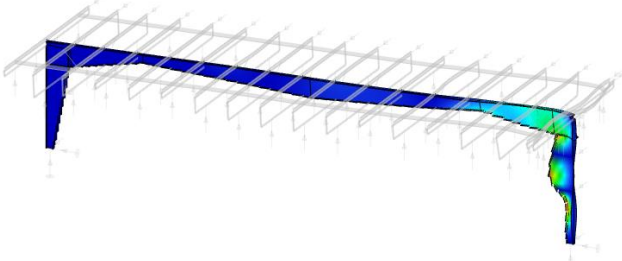


Figure 12: 3D model of the example portal frame with standing seam roof panels.

Table 3: Relevant elastic buckling modes for the frame with standing-seam roof panels.

Mode	$\gamma_{e.op}$	Elastic buckling mode shape
1	2.84	
3	3.09	

9	4.55	
---	------	--

The final unity check results, considering the interaction of axial compression and major-axis bending moments are evaluated in accordance with AISC 360 Chapter H equations. The unity check results are summarized in Figure 13. As all the unity checks are close to 1.00, the strength of the structure is nearly adequate. However, a number of unity checks are slightly larger than 1.0.

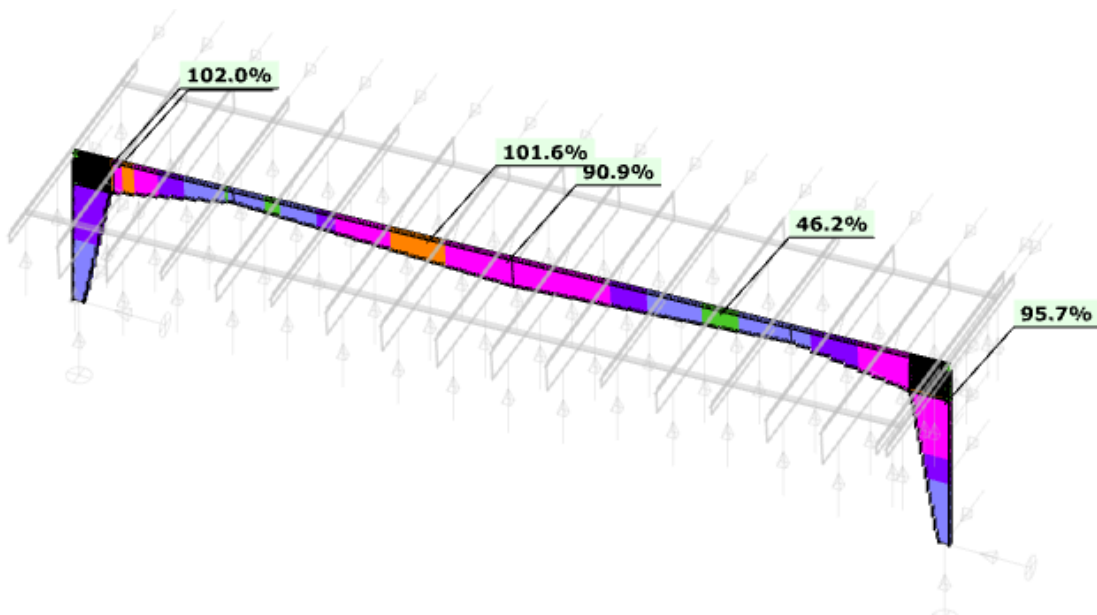


Figure 13: Final unity check results

5.3 Stabilization forces in the bracing components

As the eigenvalues of the buckling modes relevant for the design of the portal frames according to Table 2. and Table 3. are all above 2.00, the second order amplification of the brace forces is not expected to be significant. Therefore, the brace force and displacement amplification will be relatively small, and the brace forces can be assessed by simple equations as discussed in Section 4.

5.4. Discussion of results

The elastic buckling modes obtained for the standing seam option are visibly different from the ones belonging to the screwed-down roof option. This is due to the differences in the provided shear stiffness to the underlying purlins, which as a consequence provide very different lateral stabilization to the roof girder.

The most noticeable difference is that, in the case of the standing seam roof option, the rafter is less efficiently stabilized and the buckling mode corresponding to the middle part of rafter has become the lowest eigenvalue mode with an eigenvalue dropping from 4.99 to 2.84 (compare the results from Table 2. and Table 3). Not only has the relevant eigenvalue decreased significantly, but also the corresponding mode shape is completely different. The wavelength does not correspond to the purlin spacing anymore, but is much longer, due to the freedom of the purlins to displace given the low shear stiffness of the standing seam roof system (see Figure 14).

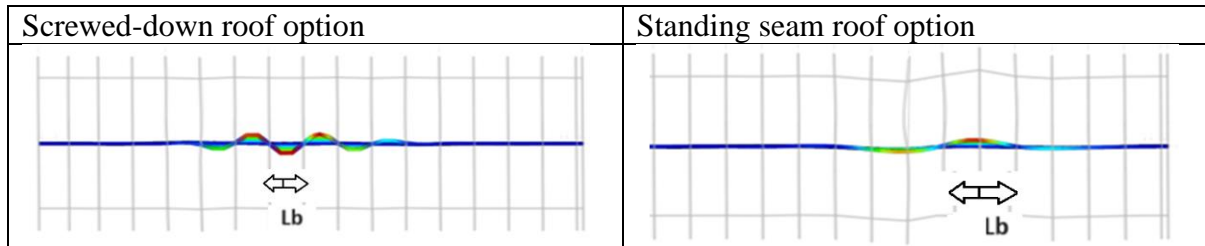


Figure 14: Representative buckling mode shapes for each of the roof types.

The example building was originally designed with a screwed-down roof option, taking the benefit of every purlin acting as an efficient lateral restraint where the upper flange of the rafter is in compression. When the standing seam option is modelled using the proposed approach, the available lateral stabilization becomes less efficient and the slenderness λ_{op} values calculated on the basis of the $\gamma_{e.op}$ values become larger. This results in a drop of the M_{nLTB} strength values close to the ridge location and gives an increase to the final unity check results from the original maximum values near 90% to some values slightly above 100%.

6. Conclusions

A complete design workflow has been presented which makes it possible to provide safe and practical design of metal building frames considering their complex bracing systems. The proposed method fulfills the intent of AISC 360 Appendix 6 while addressing the various complexities of the bracing design not addressed by the appendix.

The presented method utilizes and highlights the use of the General Method as fundamental approach for design of metal building frames and their bracing. When this method is used, it becomes possible to configure the bracing in a way that structurally best suits the standard details of metal buildings and check whether the structure considering such bracing can meet the strength requirements.

Acknowledgments

Special thanks are extended to Igor Marinovic, Senior Research Engineer at Varco Pruden Buildings, for consultations about solutions typically used for metal buildings and for the example building considered in this paper.

The US author acknowledges the fruitful discussions with colleagues and the support of various research-related endeavors by MBMA, AISC, and AISI over the years.

References

- AISC (2022). Specification for Structural Steel Buildings, ANSI/AISC 360-22, American Institute of Steel Construction, Chicago, IL.
- AISI S310 (2020) "North American Standard for the Design of Profiled Steel Diaphragm
- Consteel (2024), www.consteelsoftware.com.
- Lokhande, A.M. and White, D.W. (2015). "Evaluation of Steel I-Section Beam and Beam-column Bracing Requirements by Test Simulation" Research Report to the American Institute of Steel Construction, School of Civil and Environmental Engineering, Georgia Institute of Technology, Atlanta, GA.
- Panels, 2016 Edition" (2020). AISI-Specifications for the Design of Cold-Formed Steel Structural Members.
- Phillips, M., Kamath, A.M., Sherman, R.J., White, D.W. (2023b). "Influence of web distortion and onset of yield on doubly symmetric built-up I-girders subjected to high moment gradient," *Thin-Walled Structures*, 185, doi/10.1016/j.tws.2023.110545.
- Phillips, M., Slein, R., Sherman, R.J., White, D.W. (2023a). "Experimental investigation of doubly-symmetric built-up I-girders subjected to high moment gradient," *Engineering Structures*, Volume 283, 2023, doi.org/10.1016/j.engstruct.2023.115724.
- Prado, E.P. and White, D.W. (2015). "Assessment of Basic Steel I-Section Beam Bracing Requirements by Test Simulation," Research Report to the American Institute of Steel Construction, School of Civil and Environmental Engineering, Georgia Institute of Technology, Atlanta, GA.
- Reichenbach, M., White, J., Park, S., Zecchin, E., Moor, M., Liu, Y., Liang, C., Kovesdi, B., Helwig, T., Engelhardt, M., Connor, R., and Grubb, M. (2021). "Proposed Modifications to AASHTO Cross-Frame Analysis and Design," NCHRP Research Report 962.
- Simulia (2024). Abaqus 6.13, Dassault systems.
- Slein, R., Kamath, A.M., Phillips, M., Sherman, R.J., Scott, D.W., White, D.W. (2023). "Experimental and analytical assessment of the LTB resistance of built-up steel I-section members," *Journal of Constructional Steel Research*, doi/10.1016/j.jcsr.2022.107771.
- Szalai, J. (2011a). "The 'General Method' of EN 1993-1-1," *NSC*, April, 30-31.
- Szalai, J. (2011b). "Practical application of the 'general method' of EN 1993-1-1," *NSC*, May, 30-32.
- Szalai, J. (2017). "Complete generalization of the Ayrton-Perry formula for beam-column buckling problems" *Engineering Structures* 153, 205-223.
- Vaszilievits-Sömjén, B., Szalai, J. and White, D.W. (2023). "Frame Design Using Nonprismatic Members – Satisfying the Need for Speed", Proceedings of the Annual Stability Conference Structural Stability Research Council Charlotte, North Carolina, April 11-14, 2023.
- Wei, G. Schafer, B.W., Seek, M., and Eatherton, M.R. (2020) „Expertimental study on the in-plane behavior of standing seam roof assembly and its use in lateral bracing of rafters”. Cold-formed Steel Research Consortium REPORT SERIES CFSRC R-2020-02
- White, D.W., Jeong, W.Y. and Slein, R. (2021) Design Guide 25: Frame Design Using Nonprismatic Members, Second Edition, AISC/MBMA.
- White, D.W., Sharma, A., Kim, Y.D. and Bishop, C.D. (2011). "Flange Stability Bracing Behavior in Metal Building Frame Systems," Final Research Report to Metal Building 286 Manufacturers Association, Structural Engineering, Mechanics, and Materials Report No. 11-74, School of Civil and Environmental Engineering, Georgia Institute of Technology, Atlanta, GA, 361 PP.
- Yura, J.A. (2001). "Fundamentals of Beam Bracing," *Engineering Journal*, AISC, 38(1), 11-26.